



Development of biodegradable magnesium alloy stents with coating

Lorenza Petrini

Civil and Environmental Engineering Department, Politecnico di Milano, Italy)

lorenza.petrini@polimi.it

Wei Wu, Dario Gastaldi, Lina Altomare, Silvia Farè, Francesco Migliavacca

Chemistry, Materials and Chemical Engineering 'Giulio Natta' Department, Politecnico di Milano, Italy

wei.wu@polimi.it, dario.gastaldi@polimi.it, lina.altomare@polimi.it, silvia.fare@polimi.it, francesco.migliavacca@polimi.it

Ali Gökhan Demir, Barbara Previtali, Maurizio Vedani

Department of Mechanical Engineering, Politecnico di Milano, Italy

aligokhan.demir@polimi.it, barbara.previtali@polimi.it, maurizio.vedani@polimi.it

ABSTRACT. Biodegradable stents are attracting the attention of many researchers in biomedical and materials research fields since they can absolve their specific function for the expected period of time and then gradually disappear. This feature allows avoiding the risk of long-term complications such as restenosis or mechanical instability of the device when the vessel grows in size in pediatric patients. Up to now biodegradable stents made of polymers or magnesium alloys have been proposed. However, both the solutions have limitations. The polymers have low mechanical properties, which lead to devices that cannot withstand the natural contraction of the blood vessel: the restenosis appears just after the implant, and can be ascribed to the compliance of the stent. The magnesium alloys have much higher mechanical properties, but they dissolve too fast in the human body. In this work we present some results of an ongoing study aiming to the development of biodegradable stents made of a magnesium alloy that is coated with a polymer having a high corrosion resistance. The mechanical action on the blood vessel is given by the magnesium stent for the desired period, being the stent protected against fast corrosion by the coating. The coating will dissolve in a longer term, thus delaying the exposition of the magnesium stent to the corrosive environment. We dealt with the problem exploiting the potentialities of a combined approach of experimental and computational methods (both standard and ad-hoc developed) for designing magnesium alloy, coating and scaffold geometry from different points of views.

Our study required the following steps: i) selection of a Mg alloy suitable for stent production, having sufficient strength and elongation capability; ii) computational optimization of the stent geometry to minimize stress and strain after stent deployment, improve scaffolding ability and corrosion resistance; iii) development of a numerical model for studying stent degradation to support the selection of the best geometry; iv) optimization of the alloy microstructure and production of Mg alloy tubes for stent manufacturing; v) set up, in terms of laser cut and surface finishing, of the procedure to manufacture magnesium stents; vi) selection of a coating able to assure enough corrosion resistance and computational evaluation of the coating adhesion.

In the paper the multi-disciplinary approach used to go through the steps above is summarized. The obtained results suggest that developed methodology is effective at designing innovative biomedical devices.



KEYWORDS. Bioresorbable alloys; Degradable scaffolds; Polymeric coating; Computational studies; Experimental validations.

INTRODUCTION

In the last years stent implantations (whether coronary stent or not) have steadily grown both in terms of number and of variety of implantations (type of blood vessels involved). As a consequence, a reduction in the number of surgical operations, which are more invasive for the patient (as, for example, the coronary by-pass surgery), was observed.

As known, a bare metal stent (BMS) is a metallic mesh (obtained by laser cutting of a tube made of stainless steel, titanium or cobalt alloy) that is designed to expand a stenotic blood vessel (that is a vessel clogged by atherosclerotic plaque), thus enhancing the blood flux in the downstream vessel.

During the implant the stent is fixed on the ending part of a catheter, which consists of an "inflatable balloon". The catheter is inserted in an artery through a skin cut. Once in position the balloon is inflated with a consequent dilatation of the stent, which exerts a radial force on the stenotic blood vessel. Then, the balloon is deflated and the catheter extracted: due to the permanent deformation, the stent remains in place and withstands the natural contraction of the blood vessel.

Once in the vessel, the stent is enveloped by a new tissue, called neointima. It has been observed that in some cases the neointima proliferates in an uncontrolled way (hyperplasia) and tends to re-obstruct the vessel, thus vanishing the effect of the implantation.

To avoid the neointimal proliferation, drug eluting stents (DES) have been introduced in the clinical practice from the beginning of 21st Century. They are metallic stent coated by a polymer which locally releases an anti-inflammatory drug. Recent studies claimed that in some cases DES may lead to the generation of thrombi after a long period (late stent thrombosis), which are extremely dangerous for the patient [1,2]. Moreover, they prevent late vessel adaptive or expansive remodeling, and hinder surgical re-vascularization.

For this reason, starting from the clinical consideration that vessel scaffolding is only required transiently [3], a new generation of stents is under study [4]. It consists of bioresorbable scaffolds (BRS): the stent should remain in the body for the time required to support the vessel tissues, then it "vanishes" as it is dissolved in the human body. In this way the development of inflammatory phenomena (the reason for the hyperplasia of the neointima) is largely reduced, therefore avoiding the risk of restenosis. Moreover, thanks to the fairly long lasting mechanical action, the blood vessel is remodeled and remains opened also after the stent is fully dissolved. Moreover, the vessel can recover the natural vasomotor response, reintervention is facilitated, the dual anti-platelet therapy is shorter, the risk of strut fracture-induced restenosis is reduced and mechanical instability of the device when the vessel grows in size in pediatric patients is avoided.

From the side of bioresorbable materials, they are required to be biocompatible, degradable at an appropriate rate, easy to manipulate, sterilisable and storable. From the side of bioresorbable scaffolds, different properties are required corresponding to the different phases of the vessel treatments. In the first phase of artery revascularization, BRS have to mimic DES, so they have to show good deliverability, flexibility, ductility, minimum recoil, high acute radial strength. In the second phase of restoration of the vessel natural vasomotor response, they have to perform the transition from active support to passive implant, showing structural discontinuity and radial strength loss. In the last phase of resorption, the passive implant has to benignly disappear.

Up to now biodegradable stents made of polymers or magnesium or iron alloys have been proposed [5,6]. However, all the solutions have some limitations. The polymers have low mechanical properties, which lead to devices that cannot withstand the natural contraction of the blood vessel: the restenosis appears just after the implant, and can be ascribed to the compliance of the stent. The magnesium alloys have much higher mechanical properties than polymers. Unfortunately, they dissolve too fast in the human body: the duration in a blood vessel is about few weeks and not 6-10 months, as should be to withstand the vessel remodeling. Lastly, the iron alloys degrade too slowly [7,8].

In this work we present some results of an ongoing study aimed at the development of a hybrid bioresorbable stent (HBS) made of a magnesium alloy that is coated with a polymer having a high corrosion resistance. The mechanical action on the blood vessel is given by the magnesium stent for the desired period, being the stent protected against early onset of corrosion by the coating. The coating will dissolve in a longer term, thus delaying the exposition of the magnesium stent to the corrosive environment.

We dealt with the problem exploiting the potentialities of a combined approach of experimental and computational methods (both standard and ad-hoc developed) for designing magnesium alloy, coating and scaffold geometry from

different points of views, i.e mechanical properties, corrosion, manufacturability and biocompatibility, as summarized in Fig. 1.

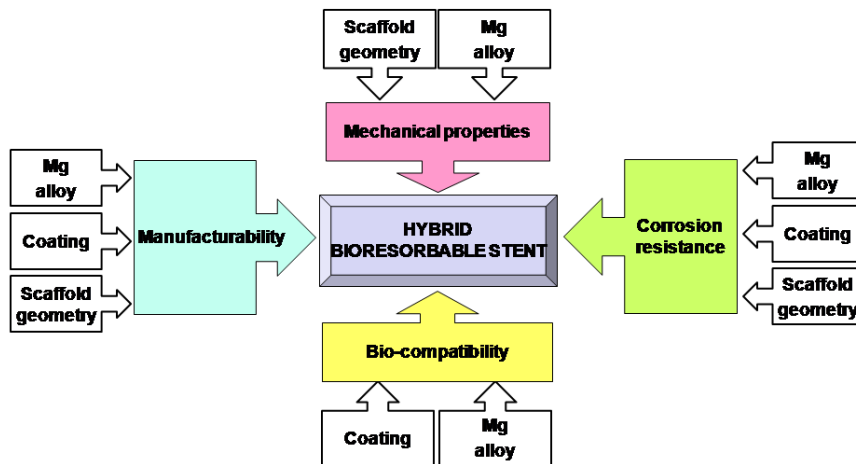


Figure 1: Scheme of the multidisciplinary approach used to develop a hybrid bioresorbable stent, made of a magnesium alloy coated with a polymer.

Up to now we performed the following steps: i) selection of a Mg alloy suitable for stent production; ii) computational optimization of the stent geometry and experimental validation; iii) development of a numerical model for studying stent degradation to support the selection of the best geometry; iv) optimization of the alloy microstructure and production of Mg alloy tubes for stent manufacturing; v) set up, in terms of laser cut and surface finishing, of the procedure to manufacture magnesium stents; vi) selection of a coating able to assure enough corrosion resistance and computational evaluation of the coating adhesion.

In the following sections, the above steps will be briefly summarized.

SELECTION OF THE ALLOY

A set of commercially available wrought Mg alloys were initially investigated. The AZ31, AZ61, AZ80, ZM21, ZK61 and WE43 alloys were considered in the form of extruded bars with a diameter of 15 mm. Specimens for tensile tests were machined from the bars with a gauge length of 40 mm and a diameter of 8 mm. Tests were performed at room temperature with an engineering strain rate of $1.3 \cdot 10^{-3}$ s⁻¹. Fig. 2 (left) depicts the tensile curves of the materials. All the alloys have a limited ductility if compared with stainless steels and Cr-Co alloys commonly used for stent production. This corresponds to a potential risk of fracture during crimping and expansion of the stent. The ZM21, AZ31 and AZ61 alloys shows the highest elongation to fracture values.

Preliminary in vitro weight loss tests were also conducted on five of the alloys (AZ31, AZ61, AZ80, ZK60 and ZM21). Cylindrical specimens (height 5 mm, diameter 10 mm for ZK60 and 14 mm for the other alloys) were polished down to 600 grit, rinsed in distilled water, degreased ultrasonically with anhydrous ethanol for 5 min and dried with warm air. The samples were immersed in a solution simulating plasma (Kokubo-c-SBF at 37 °C [9]), changed every 24 h to prevent saturation and to keep the pH to acceptable values (pH = 7.4). The surface area/solution volume ratio was 0.2 cm⁻¹.

The results plotted in Fig. 2 (right) show the best behaviour of the AZ series alloys over the ZM and ZK materials. Considering that a high percentage of aluminum may induce biocompatibility problems, AZ31 and ZM21 were selected as potential candidates for HBS and used in the following steps of stent development.

OPTIMIZATION OF THE SCAFFOLD GEOMETRY

Considering the limited ductility of the selected alloys, a shape optimization method for two HBS, made of AZ31 and ZM21 alloy respectively, was proposed. A new stent concept (Fig. 3 left) was developed with the help of a classical topology optimization procedure [10]. The design has five rings connected by curved links, presenting six



peak-to-valley struts in the circular direction. The dimensions of the outer diameter (1.4 mm) and thickness (0.15 mm) were arbitrarily fixed equal to those of an existing Mg alloy stent. A shape optimization procedure was applied to the two-dimensional (2D) model of the new design concept to minimize stress and strain after stent deployment and to improve scaffolding ability. Considering the fact that in an optimization process requires to run many analyses, the use of a 2D model is extremely beneficial, allowing to save lots of simulation time. Moreover, it is recognized in the literature that a 2D stent model can well represent the corresponding 3D model [11,12] and in this case it was verified that differences in the results (e.g. strain) between 2D and 3D expansion simulations were acceptable (less than 10%). Only one strut unit (Fig. 3 right) was chosen for optimization owing to the highly symmetrical design. A morphing procedure was used to change the strut unit shape: a few nodes at the edges of a domain (all the elements) were set as handles to control the change of the shape. An optimization algorithm based on the adaptive response surface method [13] was applied to control the shape evolution. During the procedure finite element (FE) analyses were performed on two 2D models (same design but different materials) transferred from the parametric CAD: a vertical displacement was applied to the end of the curved part of the strut to simulate the expansion of the three-dimensional (3D) stent model to an outer diameter of 3.0 mm.

The two main optimization objectives for a magnesium alloy stent are minimizing maximum principal strain, to avoid fracture, and maximizing mass or strut width, to extend the corrosion time and provide adequate scaffolding. However they are contradictory because more material may increase the strain during expansion. Accordingly, a two-step strategy was applied to find a proper design comprising the main objectives. First, only the maximum strain was minimized. In particular a solution was found when the maximum principal strain was below the 80% of the fracture strain. Second, the design with maximum normalized mass was chosen as an optimized design from optimization iterations whose maximum principal strains were below the fixed limit. The optimized design is pictured in Fig. 3. For more details about the optimization process refer to [14].

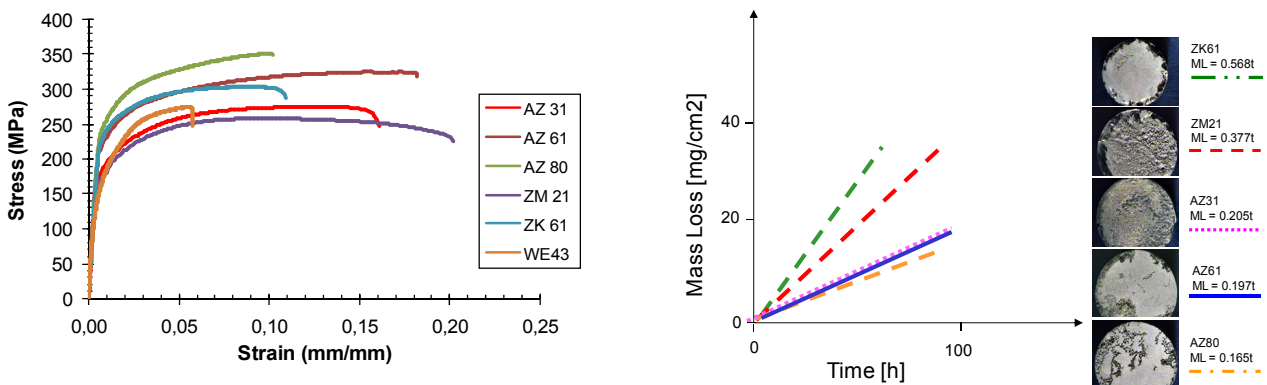


Figure 2: On the left: Tensile curves of the selected magnesium alloys. On the right: mass loss (ML) versus time curves of the studied alloys obtained from immersion tests and corresponding ML values and optical images of the specimens observed after 90h.

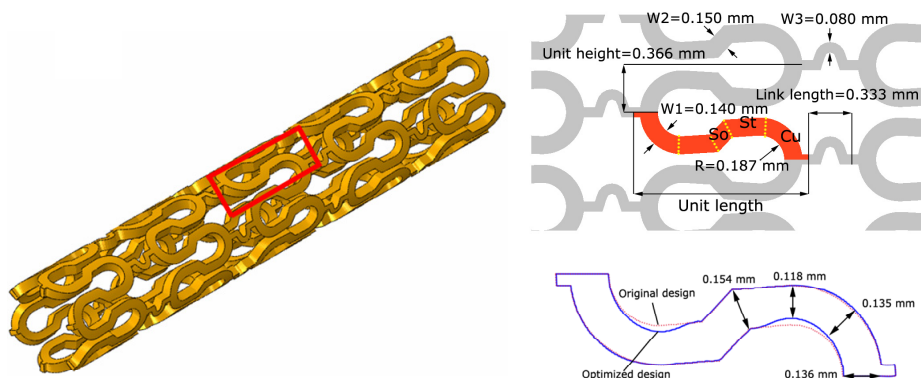


Figure 3: On the left: CAD model of the new conceptive stent in the original configuration. In the box is indicated the one strut unit chosen for the optimization. On the upper right: 2D dimensions of the new conceptive stent. In red the strut unit for optimization. The unit is composed of curved (Cu), straight (St), and solidus (So) parts. On the lower right: optimized vs original design for ZM21 alloy stent.

For a preliminary validation of the obtained results, 2D magnesium specimens having the geometry of the original and optimized models were manufactured by laser cut and experimentally tested for fracture. The original design broke at the lower displacement than the optimized design and in the locations corresponding to stress concentrated area in the simulations, showing that the optimized design was safer than the original one during expansion (Fig. 4).

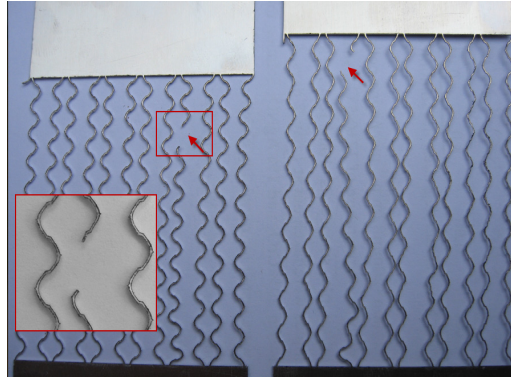


Figure 4: Comparison of the two 2D samples after fracture test: the original design (left) ruptured at lower elongation than the optimized one (right).

A DAMAGE MODEL FOR DESCRIBING STENT DEGRADATION

Aiming to develop a methodology that allows to select among different geometries the most suitable in terms of corrosion with a limited use of experimental tests, a numerical model was developed into the frame of continuum damage approach. Accordingly, a corrosion damage parameter is introduced to reflect in a phenomenological way the reduction of mechanical properties of materials. Two corrosion mechanisms are considered to attack the material in a cooperative way: uniform corrosion damage D_U , which accounts for the mass loss when exposed to a corrosive environment [15]; and stress corrosion damage D_{SC} , which describes the localized corrosion attacks in areas of the material where the stress is more concentrated [16]. The global corrosion damage variable (D) is assumed to be a linear superposition of the two mechanisms. A value of D of 0 means that the element is intact; when D equals 0.9, the element is completely damaged and will be deleted from the model during the simulation.

The damage evolution law for uniformly distributed corrosion is:

$$\dot{D}_U = \frac{\delta_U}{L_e} k_U$$

where the notation dotted D_U represents the time derivative, k_U is a parameter related to the kinetics of the process and δ_U is a characteristic dimension of the uniform corrosion process (e.g. the critical thickness of the corrosion film).

The damage evolution law for stress corrosion is [17]:

$$\dot{D}_{SC} = \frac{L_e}{\delta_{SC}} \left(\frac{S \sigma_{eq}^*}{1-D} \right)^R \quad \text{when } \sigma_{eq}^* \geq \sigma_{th} > 0$$

$$\dot{D}_{SC} = 0 \quad \text{when } \sigma_{eq}^* < \sigma_{th}$$

where σ_{eq}^* is an equivalent stress governing the stress corrosion mechanism: in this model the maximum principal stress is adopted assuming that the corrosion rate is higher at tensile stressed regions. σ_{th} corresponds to the equivalent stress value below which the stress corrosion process does not occur: in this model σ_{th} is assumed equal to 50% of the yield stress [18]. S and R are constants related to the kinetics and δ_{SC} is a characteristic dimension of the stress corrosion process.

For a proper reduction of mesh sensitivity phenomena, a direct dependency of damage evolution on the characteristic FE length L_e has been assumed. In particular, the ratio L_e/δ has been adopted in the evolution law to scale the numerical grid characteristic length over a relevant characteristic dimension of the corrosion process. See [19] for a detailed description

of the model and the used parameters. The model was implemented into a FE framework using the commercial code ABAQUS/Explicit (Dassault Systemes Simulia Corp., RI, USA) by means of a user subroutine (VUSDFLD) devoted to calculation of the damage increment through the evolution law affecting the updated stress state in the explicit time integration scheme. It was used to compare the corrosion behavior of the optimized stent (OPT) and of a patented stent (PAT) from Institute of Metal Research, CAS, Shenyang, China [20], both based on the magnesium alloy AZ31. To reduce the simulation time, we took advantage of the geometrical repetition of stent designs and we built the 3D FE models of only one ring of the two designs (Fig. 5). Aiming to study the stent degradation process taking into account the stress distribution due to implantation, we simulate all the steps of the procedure: stent crimping, balloon expansion, balloon deflating and stent recoil, stent-vessel interaction. Finally the degradation process was simulated. The details of the FE analyses are reported in [21]. It was observed that the element deletion occurred first at simulated locations of concentrated high stresses for both the designs: assumed the relative time t^* equal to 1 when both the stents lacked their structural integrity, the stress corrosion started at t^* equals 0.19, while the uniform corrosion evolved at the outer surfaces throughout the whole degradation process. PAT had a fast stress corrosion concentrated near the bows: when t^* equals 0.57, the structure was severely damaged and lost its structural integrity at t^* equal to 0.7. OPT kept more uniform stress corrosion: at t^* equals 0.95, all elements at the original outer surface were deleted and some locations were severely damaged; however, the stent still conserved its structural integrity.

To verify the FE analysis results, an experimental test was performed. The details are presented in [22]. For each design, six stent samples were manufactured by laser cut of AZ31 tubes. After stent crimping and expansion, all the 12 samples were immersed in DHanks' solution to test for degradation according to ISO 11845:1995. It was verified that under the same degradation conditions, the OPT samples keep the structural integrity longer than the PAT samples and that the degradation of the stent samples effectively includes uniform and stress corrosion. The model was able to predict the locations of sample fractures, corresponding to the locations with high residual stress. In Fig. 6 two broken samples and the corresponding simulation results are shown.

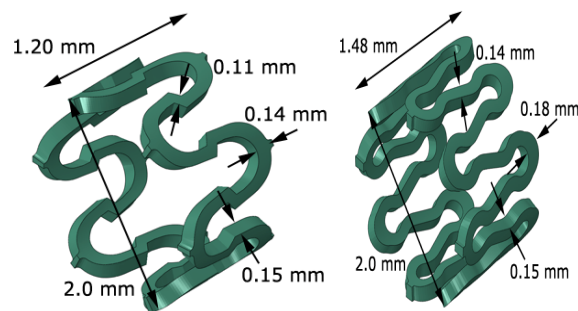


Figure 5: One ring 3D FE models of the optimized stent (left) and the patented stent (right) used in the degradation process simulations.

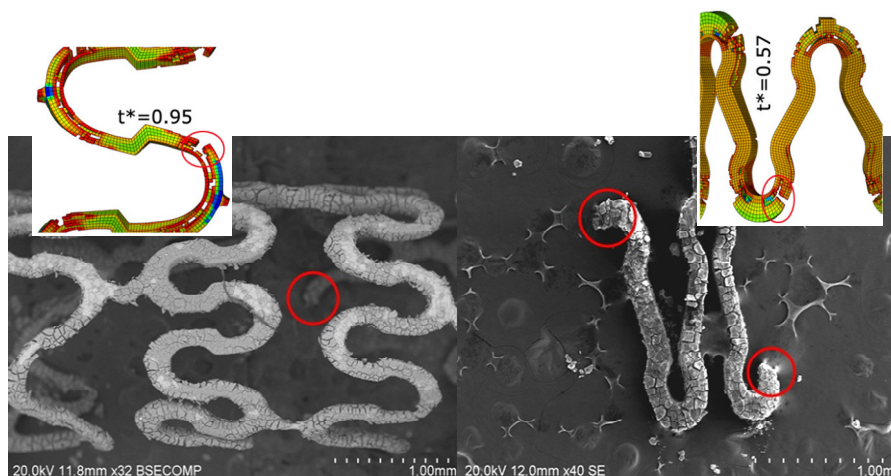


Figure 6: Experimental and numerical results of the corrosion tests of the optimized stent (left) and the patented stent (right).



ALLOY OPTIMIZATION AND TUBE PRODUCTION

Once the magnesium alloys were selected after considerations about mechanical, corrosion and toxicity properties, an optimization of the manufacturing process was performed to control microstructure and final properties of the material after production of the mini-tube by hot deformation and cold drawing, laser cutting and chemical etching of the net for the stent.

After a detailed analysis of the texture effects on design of BRS [23], we aimed to obtain a bulk ultrafine-grained (UFG) alloy in order to be able to exploit its enhanced properties: i) improved strength by marked reduction of grain size; ii) improved formability by possible superplastic properties; iii) improved mechanical behavior by modification of texture and removal of basal texture; iv) improved corrosion resistance by break-up of second-phase particles and a more homogeneous microstructure. Moreover in miniaturized devices, the specific orientation of single grains facing geometrical stress raisers leads to uncontrolled variability of device strength. On the contrary, finer grains on the cross section of the strut are expected to give a more homogeneous mechanical performance and reduce the random orientation effect given by coarse crystals.

Among the several methods based on severe plastic deformation that can be used to achieve an UFG structure in metals, the equal channel angular pressing (ECAP) was selected having the advantage of producing billets with size compatible for further extrusion of mini-tubes for stent manufacturing. After some studies, it was defined as optimal strategy for ECAP a preliminary processing at 200-250°C and then further refinement at 150-100°C. As an example, for ZM21 alloy 8 passes at 200°C 8 passes at 150°C were selected and allowed to pass from an average grain size of 15 μm for annealed material to a size of 0.52 μm after ECAP at 150°C (Fig. 7 left).

To produce stent precursors, an ad hoc set-up was developed. Extrusion was performed at 150°C, at relatively low strain rate of $3 \times 10^{-3} \text{s}^{-1}$ maintaining ultra fine grain structure. As final products, tubes having a diameter of 2.5 mm and wall thickness of about 0.2 mm were obtained (Fig. 7 right).

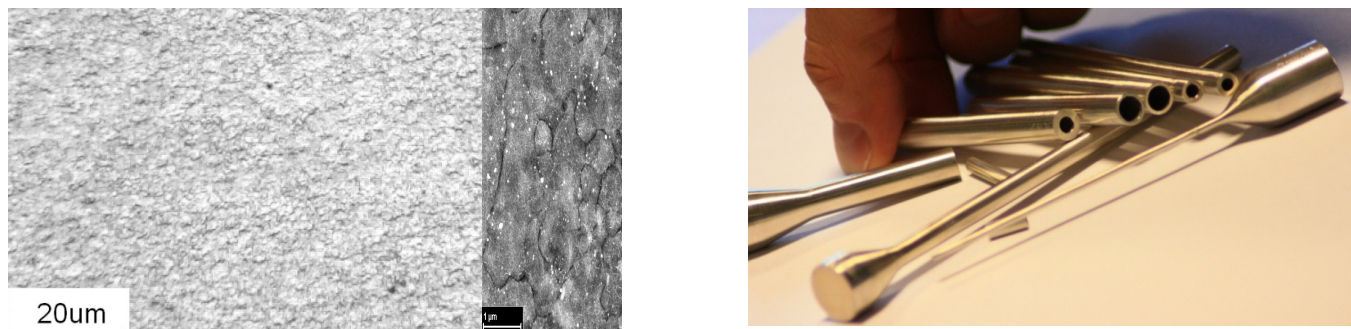


Figure 7: On the left: UFG of ZM21 alloy after ECAP; on the right: stent precursors

THE STENT PRODUCTION

The mesh of the OPT stent was cut on AZ31 tubes extruded as described above with an active fiber laser operating in ns pulse regime with 50 W maximum average power (IPG- YLP-1/100/50/50). In Tab. 1 the main characteristics of the laser source are reported. A cutting head (LaserMech) that housed a 60 mm focusing lens and a nozzle for process gas addition was used with the laser source. The calculated beam diameter in this configuration was 23 μm , which allowed microcutting with small kerf widths. The positioning system consisted of a linear and a rotary axis (Aerotech ALS and ACS series) with nanometric resolution. Laser cutting was applied with 7.5 W average power, 25 kHz of pulse repetition rate and argon as assist gas with 7 bar pressure (purity 99.998%), and cutting speed of 2 mm/s was employed. Chemical etching with an acidic solution of HNO_3 (65% purity) 10 mL, ethanol 90 mL was preferred to remove dross and to clean the kerf. The chemical operation was employed to complete separation of the stent mesh from the scrap pieces as well as to provide strut polishing [24]. The AZ31 stent after chemical etching is reported in Fig. 8. It can be seen that the stent surface is clearly free of defects. The mesh design has been reproduced with high precision on the tube. However, the stent walls show high roughness compared to the stent surfaces, which implies that further chemical polishing is required. The high corrosion rate of AZ31 in the chemical etching solution may cause excessive



etching of the stent body resulting in deviations from the stent geometry. The laser cutting quality consequently changes the final quality of the stent mesh after chemical etching. Through a comparative analysis the use of fs pulsed laser has showed an excellent compromise between surface quality after laser cutting and ease of dross reduction with chemical etching [25]. Although, today they are not highly diffused, the use of ultra-fast lasers in the industry is expected to increase in future if the capital and operational costs are reduced.



Figure 8: Optical microscopy image of the AZ31 after chemical etching.

IPG YLP-1/100/50/50 Q- switched laser	
Laser wavelength	1064 nm
Maximum average power	50 W
Maximum pulse energy	1 mJ
Minimum pulse duration [FWHM]	100 ns
Pulse repetition rate	20-80 kHz
Beam quality factor (M^2)	1.7
Focused laser beam diameter	23 μm
High precision positioning system	
Spindle accuracy	$\pm 72.7 \mu\text{rad}$
Linear axis accuracy	1 μm

Table 1: Main specifications of the laser source for stent cutting.

COATING SELECTION AND ADHESION STUDY

Among polymers commonly employed for stent coatings, such as polylactide (PLA), polycaprolactone (PCL) and polyglycolide (PGA), we investigated the potentialities of PCL for HBS production. A rotating confined dip coater was developed. Different experimental tests were performed to optimize the coating procedure of PCL on small plates in AZ31 alloy. Different speeds of immersion and extraction of the plates, different number of layers and different concentrations of PCL dissolved in chloroform or dioxane and tetrahydrofuran (THF) 1:2 ratio, were considered. Finally a concentration of PCL in chloroform equal to 1,5% w/v, a rotation speed of 300 rpm and a withdrawal speed of 150 mm/min were selected, obtaining a smooth substrate with values of thickness ranging between 5 and 10 μm .

Previous studies revealed that peeling phenomenon (or coating delamination) sometimes occurs for coated stainless stents during stent expansion [26]. If this happens to HBS, it will lead to premature corrosion onset: indeed, the corrosion will concentrate at the unprotected location and the attack will accelerate the damage of the structure. Aiming to set up a methodology that allows to select among different coatings the most suitable one in terms of adhesion properties with a limited use of experimental tests, the numerical tools available in the literature to analyze crack initiation and propagation

of surface-bonded structures were investigated. In particular FE simulations of the expansion of the HBS were performed exploiting the cohesive zone method [27] implemented in the commercial code ABAQUS.

Among the broad set of cohesive element features offered by ABAQUS, in this study, a triangle traction-separation law was chosen. Under traction deformation, the cohesive element will resist the separation between the connected surfaces with a linearly increased traction stress (along nominal stiffness K_{eff}). When the traction stress reaches the maximum limit T_{ult} (with the separation distance δ_0), the damage occurs and the traction stress decreases with further separation. At the same time, a scalar damage variable D_c , which records the damage of the cohesive element, increases starting from 0. When the element finally fails with separation δ_f , the traction stress reduces to 0 and D_c accumulates to 1. The area under the curve represents the critical energy release rate G_c .

To calibrate the cohesive element method and to measure G_c , peeling experiments were carried out for the PCL coating on the magnesium plates. The PCL was dissolved in chloroform at a concentration of 5% w/v and was dropped onto AZ31 foils (70mm x 4mm x 0.8mm). Samples were left under a hood for 24 hours to allow the complete solvent evaporation and a uniform PCL coating with a thickness of 0.01 mm was obtained. A 90-degree peeling test was carried out by a MTS Synergie 200H testing machine (MTS Systems Corporation, Minneapolis, MN,USA). Three samples were tested.

G_c was evaluated through experimental results using the formula below [28]:

$$\dot{G}_c = \left(\frac{F}{b}\right)^2 \frac{1}{2hE} + \frac{F}{b}(1 - \cos\theta)$$

where θ and F are the angle and force of peeling, b is the width, h the thickness and E the Young modulus of the coating. The FE model used to simulate the peeling tests is reproduced in Fig. 9 (left). According to the penalty parameter method proposed in [29], known G_c , other model parameters were obtained once defined δ_f . A sensitivity analysis was performed varying the value of δ_f and of the mesh-relative cohesive ductility ratio, $\delta_f/\Delta L$, being ΔL the characteristic length of the mesh. The same mesh density was used for the cohesive elements (2-dimensional, 4 node, cohesive element type COH2D4) as for the coating elements (2-dimensional, 4 node, element type CPE4R), as shown in Fig. 9 (right). The quantity selected for comparing different meshes were the adhesion force, in terms of mean value (compared with the experimental results) and the oscillation around this value (noisy solution due to “zipper effect”[29]). After these analyses, an average mesh length (mesh density) of 0.0075 mm and a key penalty parameter δ_f of 0.008 mm were selected, showing a good match with the experimental data and independency of the numerical results from the mesh size (result difference less than 2% compared to denser meshes).

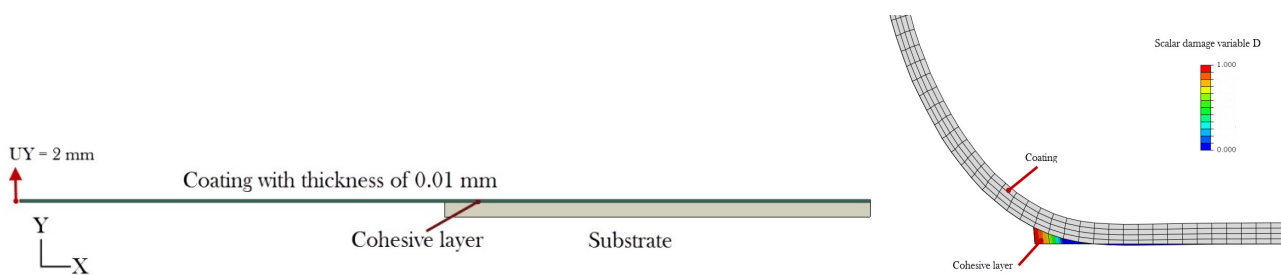


Figure 9: Finite element model of the peeling test (left); detail of the FE analysis mesh and results.

Once the method and the parameters were calibrated, the model was used to study the coated stent. The 2D strut model of OPT design with a polymer coating was modeled by finite elements. Just one side of the coating was studied because of the symmetry of the location. The thickness of the coating and of the cohesive layer was 0.01 mm and 0 mm, respectively. A symmetrical boundary condition in Y-direction was applied to one strut end and a displacement in Y-direction was applied to the other end to simulate stent diameter expansion from 2 mm to 3 mm. The mesh had a very similar element density and the same cohesive element properties as the peeling testing model (Fig. 10).

The cohesive elements were stretched after expansion, and finally failed in the inner bow of the strut when the scalar damage variable D_c of these cohesive elements reached 1 (Fig. 11 left and center). The analyses were repeated with different thickness values of the coating with the same results.

To validate the computational analysis results, stent-like 2D specimens were laser cut, subjected to chemical etching and coated by PCL, using the same technique as plate samples. The coated specimens were stretched using the same tensile

machine used for peeling tests. Peeling was detected in the bow structure of the stent strut, coherently with the simulation prediction (Fig. 11 right).

The failure of the coating was probably due to the very low adhesion force of the polymer. Accordingly some solutions are currently under evaluation: change of the polymer (PLLA), treatment of the stent surface to increase roughness, substitution of the dipping coating technique with spraying technique.

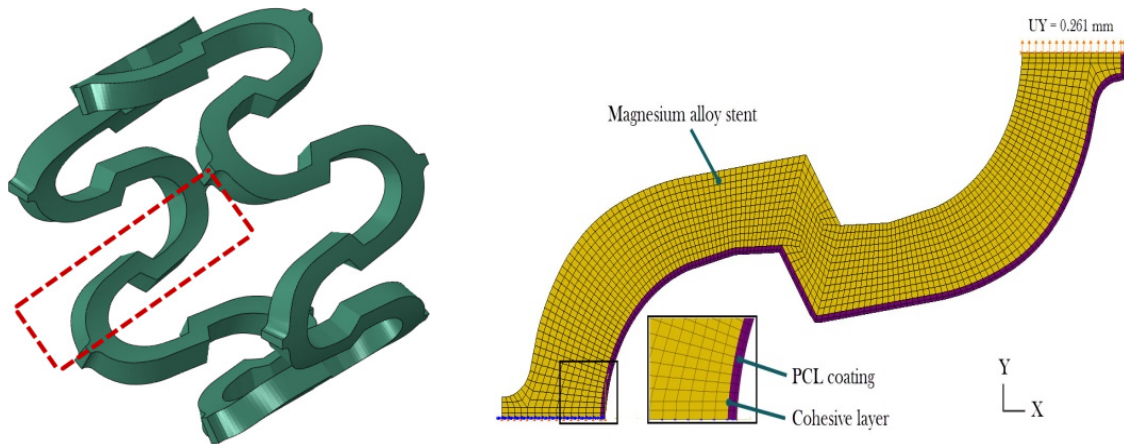


Figure 10: 3D one ring model of OPT (left) and 2D coated OPT stent strut model.

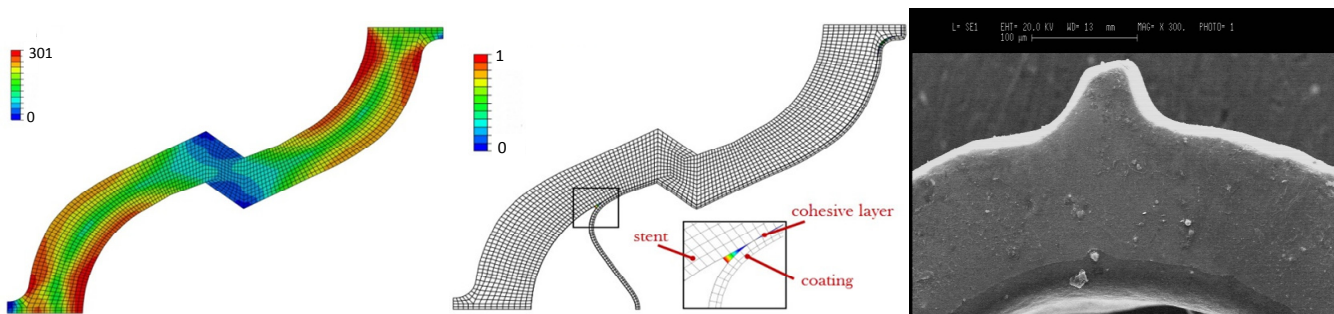


Figure 11: Numerical and experimental results of the expansion of the coated OPT stent design. Left: Von Mises stress distribution of the stent strut in MPa. Center: scalar damage variable D_c of the cohesive layer. Right: damaged coating after stent-like 2D specimen expansion.

CONCLUSIONS

A multidisciplinary approach was used to create a hybrid stent, made of magnesium alloy and coated by polymer. With the effective contribution of FE method, the development of stent has been gained in stent structure design, corrosion analysis, and coating peeling prediction. The compatible results between simulations and experiment verifications indicate that FE method is a powerful tool for magnesium stent evolution. More applications of FE method in magnesium stents are under way and the combination of simulation and experiment will be a development standard in the future.

ACKNOWLEDGEMENTS

Wei Wu is supported by the Politecnico di Milano International Fellowships Program (PIF).



REFERENCES

- [1] Tsimikas, S., Drug-eluting stents and late adverse clinical outcomes—lessons learned, lessons awaited, *J. Am. Coll. Cardiol.* 47 (2006), 2112–2115.
- [2] Wykrzykowska, J.J., Onuma, Y., Serruys, P.W., Advances in stent drug delivery: the future is in bioabsorbable stents, *Expert Opin. Drug Deliv.*, 6 (2009) 113–126.
- [3] Waksman, R., Biodegradable stents: they do their job and disappear, *J Invasive Cardiol.*, 18 (2006) 70–4.
- [4] Serruys, P.W., Garcia-Garcia, H.M., Onuma, Y., From metallic cages to transient bioresorbable scaffolds: change in paradigm of coronary revascularization in the upcoming decade?, *Eur. Heart J.* 33 (2012) 16–25b.
- [5] Carlos, C.A.M., Zhang, Y., Bourantas, C.V., Muramatsu, T., Garcia-Garcia, H.M., Lemos, P.A., Iqbal, J., Onuma, Y., Serruys, P.W., Bioresorbable Vascular Scaffolds in the Clinical Setting, *Interv Cardiol.*, 5 (2013) 639-646.
- [6] Zhang, Y., Bourantas, C.V., Takashi, V., Muramatsu, T., Diletti, R., Onuma, Y., Garcia-Garcia, H.M., Serruys, P.W., Bioresorbable scaffolds in the treatment of coronary artery disease, *Med Devices (Auckl)*, 6 (2013) 37-48.
- [7] Hermawan, H., Dubè, D., Mantovani, D., Developments in metallic biodegradable stents, *Acta Biomater.*, 6 (2010) 1693–1697.
- [8] Wiltz, C., Polymer vs. Metal: The Battle of Bioresorbable Stents, MDDI Medical Device and Diagnostic Industry News Products and Suppliers (<http://www.mddionline.com>), Oct. 2013.
- [9] Jalota, S., Bhaduri, S.B., Tas, A.C., Effect of carbonate content and buffer type on calcium phosphate formation in sbf solutions, *J. Mater. Sci. Mater. Med.*, 17 (2006) 697–707.
- [10] Wu, W., Yang, D.Z., Huang, Y.Y., Qi, M., Wang, W.Q., Topology optimization of a novel stent platform with drug reservoirs, *Med. Eng. Phys.*, 30 (2008) 1177–1185.
- [11] Donnelly, E. W., Bruzzi, M. S., Connolley, T., McHugh, P. E., Finite element comparison of performance related characteristics of balloon expandable stents, *Comput. Methods Biomech. Biomed. Eng.* 10 (2007) 103-110.
- [12] Mori, K., Saito, T., Effects of stent structure on stent flexibility measurements, *Ann. Biomed. Eng.*, 33 (2005) 733-742.
- [13] Wang, G.G., Dong, Z.M., Aitchison, P., Adaptive response surface method—a global optimization scheme for approximation-based design problems, *Eng. Optimiz.*, 33 (2001) 707–733.
- [14] Wu, W., Petrini, L., Gastaldi, D., Villa, T., Vedani, M., Lesma, E., Previtali, B., Migliavacca, F., Finite Element Shape Optimization for Biodegradable Magnesium Alloy Stents, *Ann. Biomed. Eng.*, 38 (2010) 2829–2840.
- [15] Apachitei, I., Fratila-Apachitei, L.E., Duszczek, J., Microgalvanic activity of an Mg–Al–Ca-based alloy studied by scanning Kelvin probe force microscopy, *Scripta Mater.*, 57 (2007) 1012-1015.
- [16] Winzer, N., Atrens, A., Song, G.L., Ghali, E., Dietzel, W., Kainer, K.U., Hort, N., Blawert, C., A critical review of the stress corrosion cracking (SCC) of magnesium alloys, *Adv. Eng. Mater.* 7 (2005) 659–693.
- [17] da Costa-Mattos, H.S., Bastos, I.N., Gomes, J.A.C.P., A simple model for slow strain rate and constant load corrosion tests of austenitic stainless steel in acid aqueous solution containing sodium chloride, *Corros. Sci.*, 50 (2008), 2858–2866.
- [18] Winzer, N., Atrens, A., Dietzel, W., Song, G.L., Kainer, K.U., Stress corrosion cracking in magnesium alloys: characterization and prevention, *J. Minerals, Metals Mater. Soc.* 59 (2007), 49–53.
- [19] Gastaldi, D., Sassi, V., Petrini, L., Vedani, M., Trasatti, S., Migliavacca, F., Continuum damage model for bioresorbable magnesium alloy devices - Application to coronary stents, *J. Mech. Behav. Biomed.*, 4 (2011) 352-365.
- [20] Ren, Y., Yang, K., Zhang, B., Zheng, F., Huang, J., Xiao, K., An Absorbable Implantation Stent of Magnesium Metal, China, (2006).
- [21] Wu, W., Gastaldi, D., Yang, K., Tan, L., Petrini, L., Migliavacca, F., Finite element analyses for design evaluation of biodegradable magnesium alloy stents in arterial vessels, *Mat. Sci. Eng. B-Solid*, 176 (2011) 1733-1740.
- [22] Wu, W., Chen, S., Gastaldi, D., Petrini, L., Mantovani, D., Yang, K., Tan, L., Migliavacca, F., Experimental data confirm numerical modeling of the degradation process of magnesium alloys stents, *Acta Biomater.*, 9 (2013) 8730–8739.
- [23] Vedani, M., Ge, Q., Wu, W., Petrini, L., Texture effects on design of Mg biodegradable stents, *International Journal of Material Forming*, 7 (2014) 31-38.
- [24] Demir, A.G., Previtali, B., Ge, Q., Vedani, M., Wu, W., Migliavacca, F., Petrini, L., Biffi, C.A., Bestetti, M., Biodegradable magnesium coronary stents: material, design and fabrication, *Int. j. comput. integr. manuf.*, Published online: 20 Sep 2013. DOI: 10.1080/0951192X.2013.834475.



- [25] Demir, A.G., Previtali, B., Comparative study of CW, nanosecond- and femtosecond-pulsed laser microcutting of AZ31 magnesium alloy stents, *Biointerphases*, 9, 029004 (2014); doi: 10.1116/1.4866589.
- [26] Basalus, M.W.Z., Tandjung, K., van Westen, T., Sen, H., van der Jagt, P.K.N, Grijpma, D.W., van Apeldoorn, A.A., von Birgelen, C., Scanning electron microscopic assessment of coating irregularities and their precursors in unexpanded durable polymer-based drug-eluting stents, *Catheter. Cardiovasc. Interv.*, 79 (2012) 644-53.
- [27] Camanho, P.P., Davila, C.G., de Moura, M.F., Numerical simulation of mixed-mode progressive delamination in composite materials, *J. Compos Mater.*, 37 (2003) 1415-1438.
- [28] Kinloch, A.J., Lau, C.C., Williams, J.G., The peeling of flexible laminates, *Int. J. Fracture*, 66 (1994) 45-70.
- [29] Diehl, T., On using a penalty-based cohesive-zone finite element approach, Part I: Elastic solution benchmarks, *Int. J. Adhes. Adhes.*, 28 (2008) 237-55.